JOURNAL OF MATERIALS SCIENCE **34** (1999) 917–924

Dielectric properties of spark-plasma-sintered $BaTiO_3$

TOMONARI TAKEUCHI*, E. BÉTOURNÉ, MITSUHARU TABUCHI, HIROYUKI KAGEYAMA
Osaka National Research Institute, AIST, Midorigaoka 1-8-31, Ikeda, Osaka, 563-8577 Japan
E-mail: takeuchi@onri.go.jp

YO KOBAYASHI
Central Research Institute of Electric Power Industry, 11-1,2-chome, Iwado-Kita, Komae, Tokyo, 201-8511 Japan

A. COATS, F. MORRISON, D. C. SINCLAIR, A. R. WEST
Department of Chemistry, University of Aberdeen, Meston Walk, Aberdeen, AB24 3UE, UK

Spark-plasma-sintering (SPS) has been applied to $BaTiO_3$ to prepare dense ceramics consisting of submicrometre-sized powder. Relatively dense (typically 97% of the theoretical X-ray density) pellets with an average grain size remaining similar to that of the starting powder, approximately 0.6 μm, were obtained by the SPS process. Fixed frequency (1 kHz) measurements show the room temperature permittivity of SPS ceramics to be relatively high, approximately 3500, and at least double the value of conventionally sintered ceramics, approximately 1500. Alternating current (a.c.) impedance spectroscopy measurements show that SPS is an effective process to reduce the influence of intergranular (grain boundary) effects on the permittivity and direct current (d.c.) resistance characteristics of $BaTiO_3$ ceramics substantially.

1. Introduction

Barium titanate ($BaTiO_3$) is a well known ferroelectric material with a high room temperature permittivity value, $\geq$1000, and will continue to be used in the manufacture of thermistors, multilayer capacitors and electro-optic devices into the next century [1]. Recently, it has been extensively studied particularly for its application as a capacitor material in down-sized portable machines and dynamic random access memory (DRAM) devices [2–5]. For the above applications, $BaTiO_3$ ceramics with both high dielectric constants and high resistivity properties in small size are required.

However, drastic decrease in electrical permittivity has been reported for $BaTiO_3$ ceramics with submicrometre-sized grains [6–10]. This arises mainly because it is difficult to prepare dense $BaTiO_3$ ceramics with fine grains (<1 μm) via conventional sintering process.

Oonishi *et al.* [11] prepared dense $BaTiO_3$ ceramics (more than 98% of the theoretical X-ray density) with submicrometre-sized grains (0.2–0.6 μm) by hot isostatic pressing (HIP). They applied 500 MPa to the powders during sintering, which is enough to decrease the c/a-ratio of the tetragonal unit cell, Curie temperature and permittivity of $BaTiO_3$ ceramics [12, 13].

Spark-plasma-sintering (SPS) is a process that makes use of microscopic electrical discharge between particles under pressure (approximately 30 MPa) [14–16]. Although SPS is commonly used to produce dense metal and engineering ceramics, there are relatively few reports on the application of this technique to produce dense ceramics of oxides for electrical ceramics. The SPS process enables a compact powder to be sintered under uniform heating to high density at relatively lower temperatures and in much shorter sintering periods, typically a few minutes, compared with conventional sintering of cold-isostatic pressed (CIP) pellets [14–16]. The short sintering periods carried out for the SPS process would be advantageous in suppressing exaggerated grain growth.

Many researchers who have studied the dielectric properties of $BaTiO_3$ ceramics report only fixed-frequency measurements, e.g. permittivity and/or dissipation factor (tan δ) at 1 kHz [1]. Polycrystalline materials commonly exhibit a variety of frequency-dependent effects associated with heterogeneities, such as grain boundaries or surface layers, in addition to the intrinsic properties of the materials concerned [17]. In order to characterize the electrical properties of polycrystalline ferroelectric $BaTiO_3$ ceramics fully, Hirose and West have recently shown that a.c. impedance measurements should be made over a wide frequency range and the data analysed using a variety of formalisms [17].

In this paper, we try to produce dense pellets of $BaTiO_3$ with submicrometre grain size using the SPS process. The electrical properties of the SPS $BaTiO_3$ pellets were measured using a.c. impedance spectroscopy and the results compared with those obtained for conventionally sintered $BaTiO_3$ ceramics.

* Author to whom correspondence should be addressed.

TABLE I Synthesis methods of the starting $BaTiO_3$ powders, sintering methods and densities of the pellets (theoretical X-ray density is 6.01 g cm^{-3})

Pellet	Synthesis method of the starting $BaTiO_3$	Sintering method	Density (g cm^{-3})
SPS	Hydrolysis ($Ba(OH)_2$ + $Ti[OCH(CH_3)_2]_4$)	Spark-plasma-sintering (1100 °C 3 min)	5.80 (97)[a]
CH	Hydrolysis ($Ba(OH)_2$ + $Ti[OCH(CH_3)_2]_4$)	Conventional heating (1200 °C 2 h)	5.29 (88)[a]
SSR	Solid state reaction ($BaCO_3$ + TiO_2)	Conventional heating (1200 °C 2 h)	5.47 (91)[a]

[a]Values in parenthesis are per cent relative densities.

2. Experimental procedure

$BaTiO_3$ powders were prepared by alkoxide hydrolysis from the addition of reagent grade titanium tetraisopropoxide ($Ti[OCH(CH_3)_2]_4$; Wako Pure Chemical Industries) to 0.45 N barium hydroxide ($Ba(OH)_2$; Wako Pure Chemical Industries, reagent grade) aqueous solution at 80 °C under a N_2 atmosphere to avoid the formation of $BaCO_3$, as described previously [18, 19]. The precipitate was filtered and dried in an oven (100 °C) overnight. The as-prepared powders were calcined at 1200 °C for 4 h, leading to tetragonal $BaTiO_3$ with an average particle size of 0.6 μm [19]. These powders were subsequently sintered in the form of discs by SPS using an SPS-2040 (Sumitomo Coal Mining) or by conventional heating in a muffle furnace.

Fig. 1 shows a schematic representation of the SPS system employed. $BaTiO_3$ powder was placed into a graphite die (2 cm in diameter) and an electric current (d.c.) of 4000 A was applied under a pressure of 39 MPa. During this procedure, the temperature increased to 1100 °C at a rate of approximately 200 °C min^{-1}. Although the temperature was monitored at the surface of the graphite die by a pyrometer, the temperature difference between the graphite surface and sample interior was less than 20 °C in this system [20]. After it was maintained at 1100 °C for approximately 3 min, the applied electric current was stopped, pressure was released and the sample was cooled to room temperature (it took approximately 1 min for cooling from 1100 to 600 °C). Although the as-sintered pellets (2 cm in diameter and 0.2 cm in thickness) were black in appearance, probably due to contamination of carbon from the die and/or the reduction of the sample pellets, the white appearance of the pellets was restored by annealing in air at 1200 °C for 2 h (SPS pellets). For the conventional heating process, $BaTiO_3$ prepared by the hydrolysis method (average grain size was approximately 0.6 μm) was pressed into pellets under a pressure of 190 MPa (green density was typically 2.83 g cm^{-3}, i.e. 47% of the theoretical X-ray density) and subsequently sintered in air for 2 h at 1200 °C (CH pellets). For comparison, $BaTiO_3$ was also prepared by solid state reaction of $BaCO_3$ (Wako Pure Chemical Industries, 99.9%) and TiO_2 (Wako Pure Chemical Industries, reagent grade) at 1200 °C for 4 h (average grain size was approximately 1 μm and the Ba/Ti cation ratio was 1.00 ± 0.01 by ICP measurements). These samples were also pressed into pellets under a pressure of 190 MPa (green density was typically 2.78 g cm^{-3}, which was 46% of the theoretical X-ray density) and sintered in a muffle furnace at 1200 °C for 2 hours (SSR pellets). The synthesis method of the starting $BaTiO_3$ powders and sintering methods for the pellets are summarized in Table I.

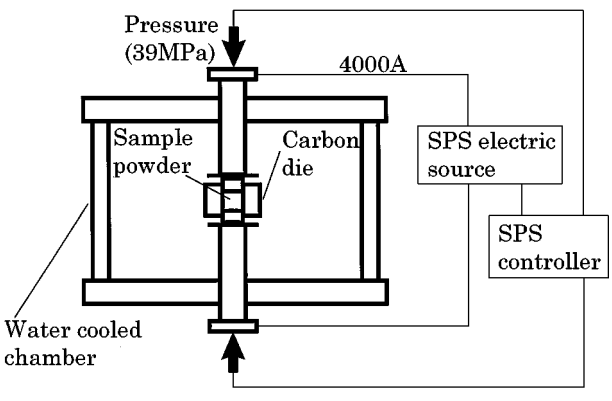

Figure 1 Schematic representation of the spark-plasma-sintering system (SPS 2040 of Sumitomo Coal Mining) employed in this study.

Phase purity and composition of the pellets were checked by X-ray diffractometry (XRD; Rigaku Rint-1500 using CuK_α radiation), scanning electron microscopy (SEM; Nikon E-SEM 2700L) with energy dispersion X-ray (EDX) microanalysis (Philips Edax DX-4), electron probe microanalysis (EPMA; Cameca SX51) and Raman spectroscopy (Jobin Yvon T64000). In the EDX system, the detector window was made from a thin polymer film, which enabled the detection of light elements such as carbon and oxygen, and the standard used for Ba and Ti analysis in EPMA was $BaTiSi_3O_9$. Thermogravimetry (Rigaku TAS200) was employed to monitor any weight changes on reoxidation of the pellets prepared from the SPS method.

A.c. impedance measurements were carried out using combined Solartron 1250/1286 and Hewlett Packard 4192A instrumentation, covering the frequency range 10^{-2}–10^7 Hz. Prior to electrical measurements, pellets were coated with Au paste electrodes (Engelhard A-3360), which were fired on at 600 °C. All samples were measured over the temperature range 25–300 °C, with equilibration periods of 15 min at each temperature.

3. Results and discussion

XRD patterns of the starting powder, and SPS pellets before and after annealing are shown in Fig. 2. The presence of graphite contamination from the carbon die in sintered SPS pellets was clearly observed in the XRD patterns; however, annealing the pellets in air at 1200 °C for 2 h was sufficient to remove graphite contamination. Lattice parameters of the annealed pellets were $a = 0.3997(5)$ nm and $c = 0.4038(6)$ nm, in good agreement with those reported previously for tetragonal $BaTiO_3$ [21] and with those of the starting powder,

TABLE II Composition for the SPS, CH and SSR $BaTiO_3$ pellets determined with EPMA

Element	SPS $BaTiO_3$		CH $BaTiO_3$		SSR $BaTiO_3$		Theoretical value for $BaTiO_3$ (at %)[a]
	Average	Standard deviation	Average	Standard deviation	Average	Standard deviation	
Ba	19.86	0.17	19.99	0.11	20.01	0.05	20
Ti	20.00	0.11	20.00	0.08	19.99	0.03	20
O	60.13	0.06	60.00	0.04	60.00	0.02	60

[a]The atomic per cent shown here is normalized to give total per cent = 100. The actual total weight per cent was 100.02 in the SPS pellet, 99.56 in the CH pellet and 99.40 in the SSR pellet. Data of ten points were averaged in determining the composition for each sample.

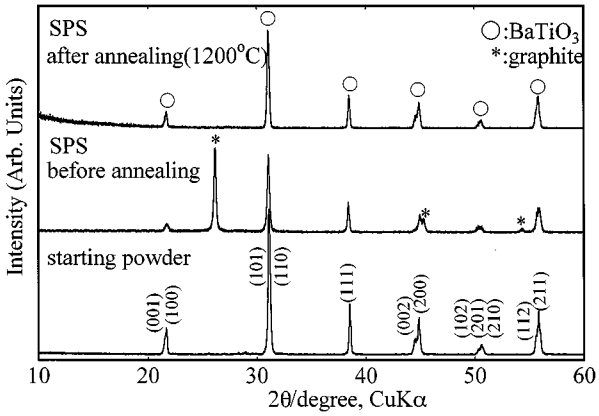

Figure 2 XRD patterns (CuK_α radiation) of the starting $BaTiO_3$ powder, and SPS pellets before and after annealing at 1200 °C for 2 h in air.

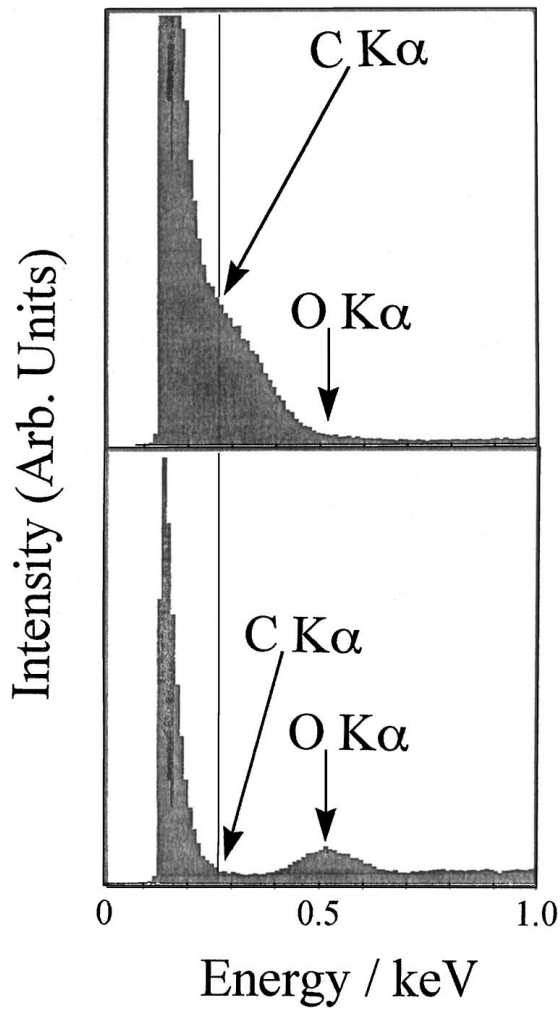

Figure 3 EDX results for SPS $BaTiO_3$ pellets before (top) and after (bottom) annealing at 1200 °C for 2 h in air.

$a = 0.3996(5)$ nm and $c = 0.4038(6)$ nm. The EDX results shown in Fig. 3 further confirm the removal of carbon contamination by annealing; the large peak at approximately 0.28 keV, attributed to the carbon K_α peak, is absent after reoxidation.

Thermogravimetry showed a weight loss of approximately 0.3 wt % on heating to 1200 °C in air, probably due to the elimination of graphite as the form of gaseous CO_2 and/or CO from the samples. SPS pellet densities remained high, typically 5.80 g cm^{-3} (97% of the theoretical X-ray density) after annealing at 1200 °C.

A typical SEM micrograph of the fracture surface of an annealed SPS pellet is shown in Fig. 4a. The SPS pellets consist of mainly submicrometre-sized grains, indicating that the average grain size remains similar to that of the starting powder, approximately 0.6 μm. In our parallel experiments for SPS at 1100 °C for 30 min, exaggerated grain growth to more than 10 μm was observed. Therefore, the short sintering period would be an essential factor to obtain $BaTiO_3$ ceramics with submicrometre-sized grains in the SPS process. For comparison, SEM micrographs of the fracture surfaces of CH and SSR pellets are shown in Fig. 4b and c, respectively. In contrast to SPS pellets, the mean grain size of both pellets increased from 0.6 to approximately 2 μm, and pellet densities were much lower, typically 5.29 (CH pellet) and 5.47 g cm^{-3} (SSR pellet) than those of the SPS pellets.

The chemical composition and homogeneity of the samples were analysed on a micrometre scale by EPMA, Table II. Although the main phase in the SPS, CH and SSR pellets was stoichiometric $BaTiO_3$, within experimental errors, small quantities of a titanium-rich (Ba : Ti ratio 1 : 2) second phase were detected as isolated grains in SPS pellets. The presence of this titanium-rich, minor phase may occur due to the loss of barium during the SPS process. This may be a reason why the compositional fluctuation and Ti/Ba ratio of the SPS pellets are slightly larger than those of the CH and SSR pellets. Raman spectra (not shown) for the SPS, CH and SSR pellets were all in good agreement with that of the characteristic tetragonal $BaTiO_3$ reported previously [22, 23], signifying negligible amounts of a nonstoichiometric phase such as $BaTi_2O_5$ [23].

Fixed-frequency, 1 kHz, permittivity data for SPS, CH and SSR pellets over the temperature range 25–300 °C are shown in Fig. 5. Although all sets show a maximum at the ferroelectric Curie temperature of approximately 120 °C, SPS data show higher permittivity values, particularly below the Curie temperature;

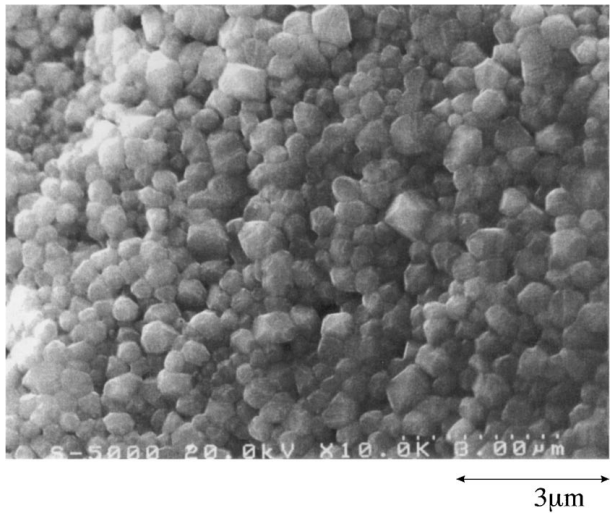

(a)

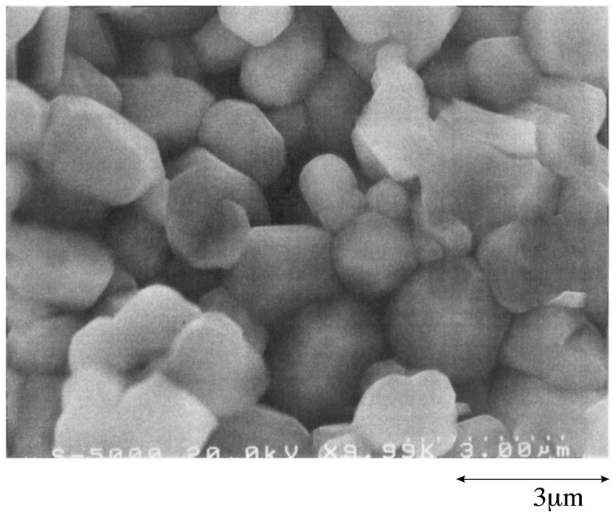

(b)

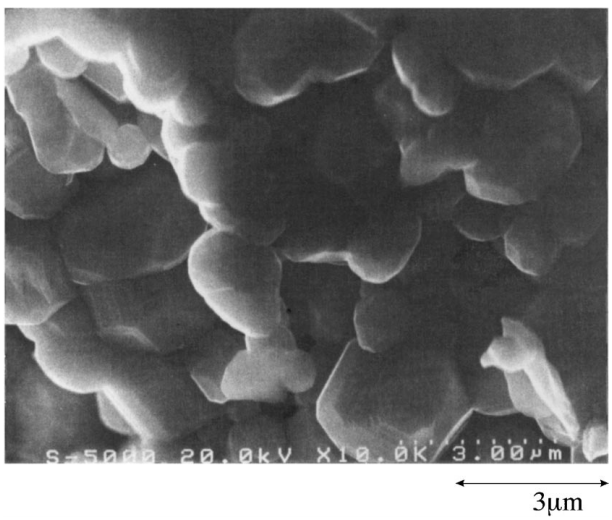

(c)

Figure 4 SEM micrographs of fracture surfaces for (a) SPS, (b) CH, and (c) SSR $BaTiO_3$ pellets.

the room-temperature permittivity of SPS pellets is approximately 3500, higher than the value for CH pellets (approximately 1500) and SSR pellets (approximately 1800). Although commercially available doped-$BaTiO_3$ shows much higher permittivity values [7], the present SPS pellets show relatively higher permittivity values in "pure" $BaTiO_3$. The dissipation factors at 1 kHz for the SPS pellets are less than 3% at 25–300 °C, which agrees with those of reported values for well sintered $BaTiO_3$ ceramics [1], suggesting less amounts of oxygen defects as well as less amounts of pores in the SPS pellets. It is well documented that the permittivity of $BaTiO_3$ ceramics depends on the grain size [6–9] and in particular that large permittivity values are obtained when the grain size is restricted to approximately 1 μm. The SPS process is clearly effective in restricting exaggerated grain growth within $BaTiO_3$, Fig. 4a, and can be used to produce dense pellets of submicrometre grain sized ceramics with relatively large permittivity values. In contrast, conventional heat processing results in porous pellets of larger grain size and consequently, lower permittivity values.

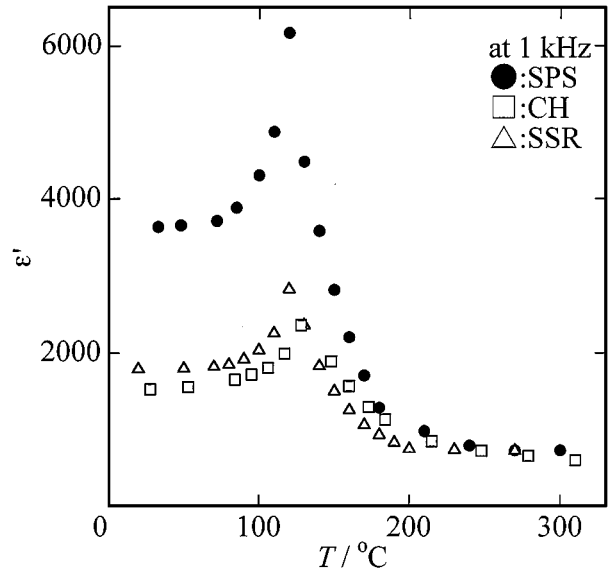

Figure 5 Temperature dependence of the permittivity at 1 kHz for SPS, CH and SSR $BaTiO_3$ pellets.

The reciprocal permittivity values at 1 kHz above the Curie temperature were plotted against temperature, Fig. 6. Data for SPS pellets showed Curie–Weiss paraelectric behaviour up to approximately 270 °C,

$$\varepsilon^{-1} = A^{-1}(T - T_0) \qquad (1)$$

where A is the Curie–Weiss constant and T_0 is the Curie–Weiss temperature. An extrapolated apparent T_0 value was approximately 108 °C, close to the reported value (approximately 115 °C) [17]. Above 270 °C deviation from the Curie–Weiss law is observed. Data for CH pellets obey the Curie–Weiss law over a narrower temperature range, i.e. between 130 and 200 °C, and give a lower extrapolated T_0 value of 98 °C. At temperatures in excess of 200 °C, gross deviation from linearity occurs. Curie–Weiss plots for SSR pellets showed similar behaviour to that observed for CH pellets.

In order to investigate the difference in ε^{-1} versus T plots of SSR, CH and SPS pellets, permittivity data were analysed as a function of frequency. Spectroscopic plots of the real component (ε') of complex permittivity ($\varepsilon = \varepsilon' + i\varepsilon''$) for SSR, CH and SPS pellets at elevated temperatures are shown in Figs 7, 8 and 9, respectively.

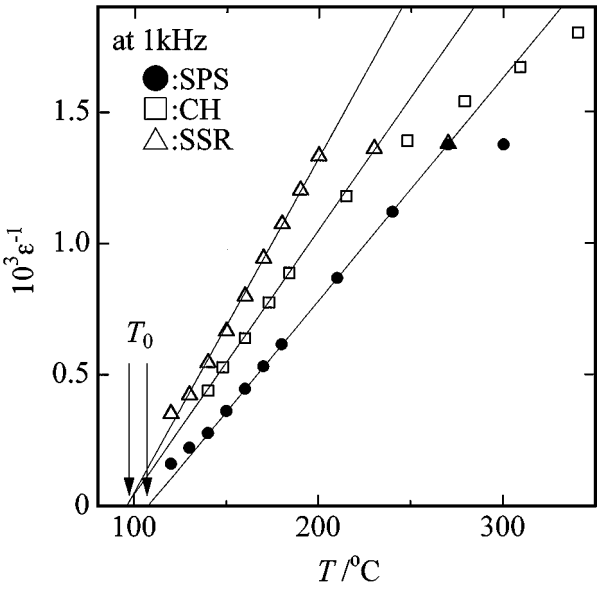

Figure 6 Reciprocal permittivity data as a function of temperature at 1 kHz for SPS, CH and SSR $BaTiO_3$ pellets. Lines indicate whether each ε'^{-1} versus T set could be fitted to a line derived from Curie–Weiss law or not.

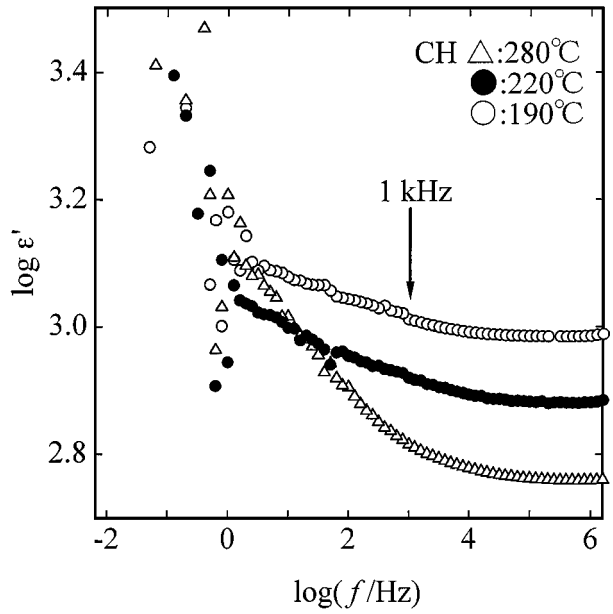

Figure 8 Frequency dependence of the real part of the complex permittivity, ε', for CH $BaTiO_3$ pellets at three temperatures. Arrow indicates 1 kHz datum point.

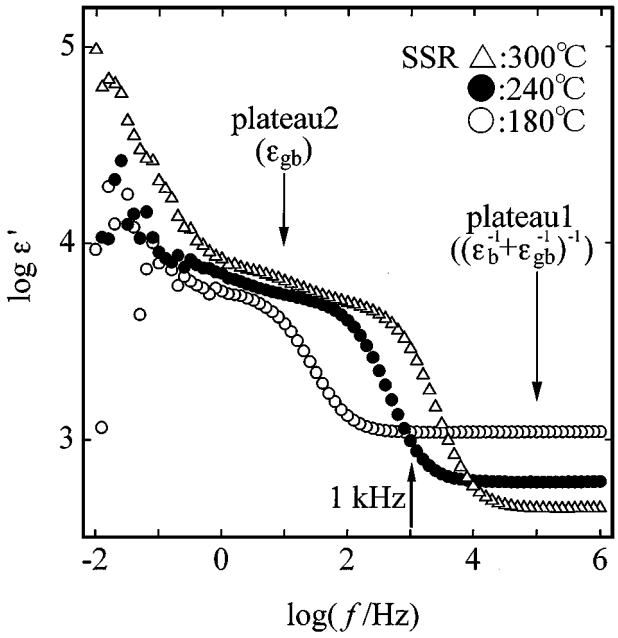

Figure 7 Frequency dependence of the real part of the complex permittivity, ε', for SSR $BaTiO_3$ pellets at three temperatures. Thickened arrow indicates 1 kHz datum point.

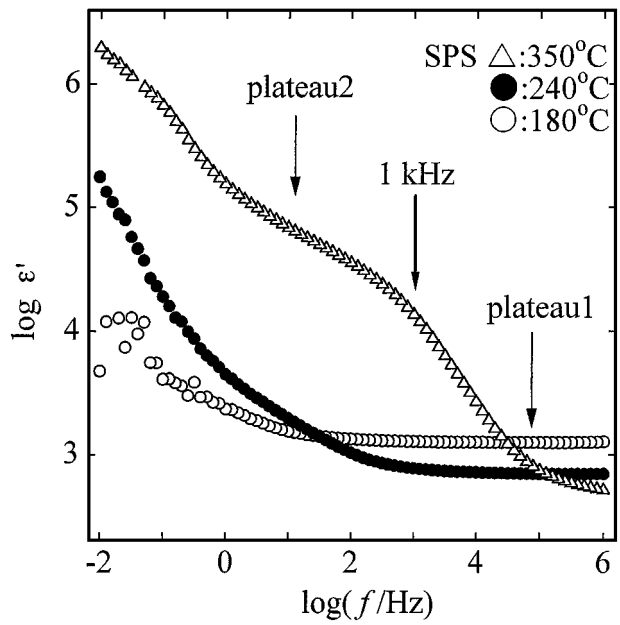

Figure 9 Frequency dependence of the real part of the complex permittivity, ε', for SPS $BaTiO_3$ pellets at three temperatures. Thickened arrow indicates 1 kHz datum point.

For SSR pellets, permittivity data reveal two distinct plateaus; with increasing temperature, spectra are displaced to higher frequencies. In contrast, data for a CH pellet at three temperatures show scatter in the low frequency region (<1 Hz) with ε' decreasing slowly at higher frequencies with no well defined high frequency plateau value. Data for SPS pellets at approximately 180 °C show clearly the presence of a high frequency plateau and at higher temperatures, e.g. >300 °C, a second, less well resolved intermediate plateau region. There appear to be no clear plateaus in the low frequency (<1 Hz) region for all samples, suggesting the absence of space-charge at the Au electrode–sample interface [24].

Hirose and West [17] have already shown that two plateau regions can be observed in ε' spectroscopic plots for conventionally sintered $BaTiO_3$ ceramics prepared from solid state reaction. Based on their model, where incompletely sintered ceramics consist of grains (of permittivity ε_b) separated by narrow, intergranular necks (of effective permittivity ε_{gb}) including air gaps, they demonstrated that the lower frequency plateau value corresponds to the permittivity of the grain boundaries, ε_{gb}, whereas the high frequency plateau value, ε_H, is a composite term containing both grain and grain boundary components, i.e.

$$\varepsilon_H = \left(\varepsilon_b^{-1} + \varepsilon_{gb}^{-1}\right)^{-1} \quad (2)$$

For most ceramic materials, the capacitance of the grain boundary component (C_{gb}, proportional to ε_{gb}) is much larger than the grain component (C_b, proportional to ε_b), and the high frequency permittivity plateau value can be approximated to the grain permittivity, ε_b, since $C_{gb} \gg C_b$. This approximation, however, cannot be used if grain capacitance values are large, as is the case for ferroelectric materials close to the Curie temperature or for poorly sintered ceramics where the grain boundary capacitance is low, such that $C_{gb} \sim C_b$.

Using this model, we can explain the fixed-frequency Curie–Weiss paraelectric behaviour and general signature of the ε' spectroscopic plots in the paraelectric region for the three types of pellets prepared in this study. The low frequency ε' plateau value in the SSR data, Fig. 7 corresponds to the grain boundary permittivity, whereas the high frequency ε' plateau is a composite value, which is dominated by the grain permittivity and is temperature dependent. Deviation in the Curie–Weiss law above 200 °C for fixed-frequency measurements on SSR pellets, Fig. 6, can be explained by the fact that in this temperature region (240 and 300 °C), 1 kHz data lie in the intermediate region between the two plateaus and are therefore an overestimation of the grain permittivity. Such ε' spectroscopic plots demonstrate that fixed-frequency 1 kHz data do not give accurate grain permittivity values for $BaTiO_3$ ceramics at moderate temperatures above the Curie temperature.

The absence of any well defined plateau in the ε' spectroscopic plots for CH pellets may be attributed to poor sintering; CH pellet densities were typically 88% of the theoretical X-ray density. The presence of large air gaps substantially reduces the capacitance associated with the grain boundary component, such that its capacitance value is similar to that of the grain response. Thus, a gradual decrease in permittivity with increasing frequency is observed, Fig. 8, rather than two, well resolved, frequency-independent plateaus associated with grain boundary and grain responses. In addition, 1 kHz fixed-frequency data become increasingly dominated by grain boundary and electrode-polarization effects with increasing temperature and account for the deviation from Curie–Weiss paraelectric behaviour above 200 °C. The low T_0 value of approximately 98 °C for CH pellets can also be explained using the model proposed by Hirose and West [17]; taking into $\varepsilon = \varepsilon_b$ in Equation 1, combining Equations 1 and 2 gives

$$\varepsilon_H^{-1} = \varepsilon_b^{-1} + \varepsilon_{gb}^{-1} = A^{-1}(T - T_0) + \varepsilon_{gb}^{-1}$$
$$= A^{-1}[T - (T_0 - A/\varepsilon_{gb})] \quad (3)$$

This equation shows that the apparent Curie–Weiss temperature is smaller than the true value, T_0, by an amount $\Delta T = A/\varepsilon_{gb}$ [17]. Porous CH pellets have lower ε_{gb} values, leading to larger shifts in ΔT and therefore lower apparent T_0 values compared with the more dense SPS pellets.

In contrast, ε' spectroscopic plots for SPS pellets show clearly the presence of a high frequency plateau above the Curie temperature and, in addition, an intermediate, lower frequency plateau at temperatures above approximately 300 °C. Due to the higher density of SPS

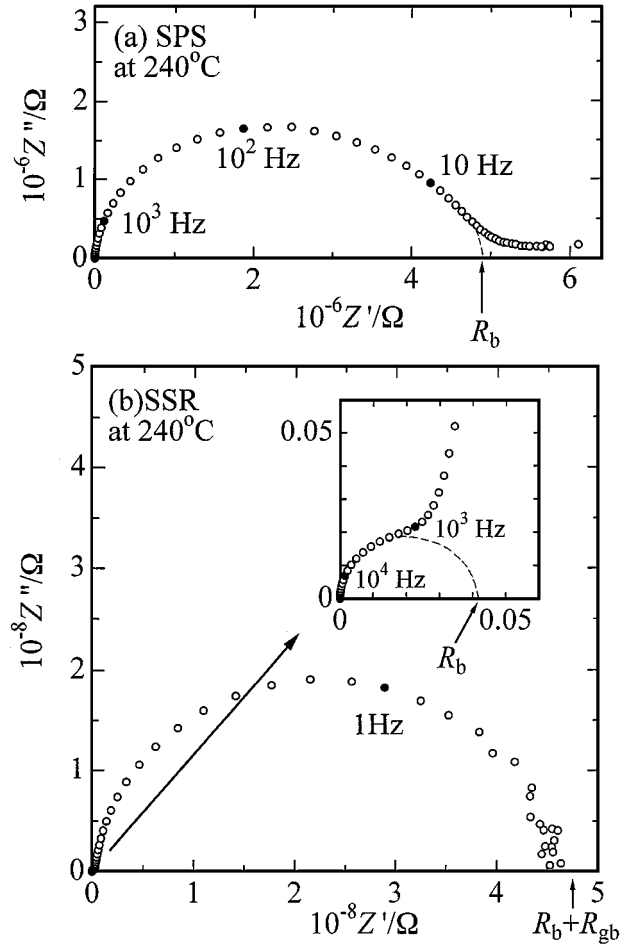

Figure 10 Impedance plane plots for (a) SPS and (b) SSR $BaTiO_3$ pellets at 240 °C. Inset shows the high frequency region for SSR pellets. Selected frequencies are shown in hertz.

pellets compared with CH pellets, ε_{gb} is larger since there are fewer air gaps, and two plateau regions are resolved. The high frequency plateau value is temperature dependent and is dominated by ε_b, since ε_{gb} is large. The 1 kHz fixed-frequency data for temperatures below 300 °C lie on the high frequency plateau, correspond to ε_b and therefore obey the Curie–Weiss law. Above 300 °C, deviations from the Curie–Weiss law occur as the 1 kHz data points lie on the intermediate region between the two plateau regions.

Representative impedance plane plots, Z^*, for SPS and SSR pellets at 240 °C are shown in Fig. 10. SPS pellets exhibit a clearly defined, high-frequency semicircular arc with an associated capacitance of 330 pF. The associated resistance (corrected for sample geometry) was 4.8 MΩ, Fig. 10a. In contrast, the overall resistance of SSR pellets is two orders of magnitude greater than that for SPS pellets at 240 °C, Fig. 10b. The impedance plane plots for SSR pellets exhibit two semicircular arcs; a large, low frequency semicircular arc with an associated capacitance of 1.7 nF, which can be assigned to a grain boundary component [17], and a small, high frequency arc, inset of Fig. 10b, with an associated capacitance of 190 pF, which can be assigned to a grain capacitance value [17]. The associated grain, R_b, and grain boundary, R_{gb}, resistances are 4.1 and 450 MΩ, respectively. Based on these two associated capacitance values of SSR pellets, the semicircular arc

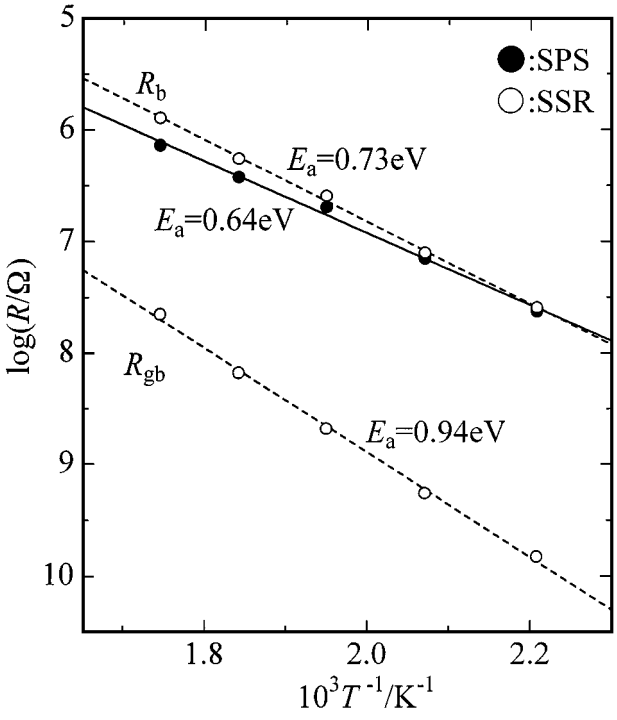

Figure 11 Arrhenius plots for R_b and R_{gb} of SPS and SSR $BaTiO_3$ pellets.

of SPS pellets can be assigned to a bulk component. The low frequency response in Fig. 10a shows evidence of a small "tail," which is associated with a small grain boundary contribution to the overall d.c. resistance of the sample.

Resistance data for SPS and SSR pellets are summarized in an Arrhenius plot, Fig. 11. There is exceptionally good agreement for the grain resistance value, R_b, and for its activation energy of both samples, 0.64 eV for SPS and 0.73 eV for SSR. This indicates clearly that the SPS process is effective in removing the high resistive grain boundary component that is commonly observed for $BaTiO_3$ ceramics prepared via conventional sintering. The activation energies for R_b in both samples are smaller than the band gap for intrinsic electronic conduction in pure $BaTiO_3$ (approximately 3 eV [17, 25]), signifying that R_b values for SPS and SSR samples are attributed to extrinsic conduction mechanisms, probably associated with minor impurities in the starting reagents. But this result cannot affect our conclusion that the SPS process is effective in removing the resistive grain boundary component of $BaTiO_3$ ceramics.

So far, we have obtained well defined stoichiometric fine $BaTiO_3$ powder by a decomposition of organometallic crystal (sol–crystal method [26]), which shows relatively high dielectric constant (3700 at room temperature [27]). Combing these two methods, i.e. sol–crystal (preparation of well defined fine powder) and spark-plasma-sintering (well sintering method), may open the possibility to produce fine $BaTiO_3$ ceramics with much higher permittivity.

4. Conclusions

We have employed spark-plasma-sintering to obtain dense $BaTiO_3$ pellets (97% of the theoretical X-ray density) with an average grain size similar to that of the starting powder, typically approximately 0.6 μm. The 1 kHz, fixed-frequency permittivity measurements show that the permittivity of SPS pellets is relatively higher than that obtained for conventionally sintered ceramics, with a typical room-temperature permittivity value of approximately 3500. A.c. impedance results demonstrate that the SPS process is effective in removing the resistive grain boundary component, which is commonly observed in conventionally sintered $BaTiO_3$ ceramics.

Acknowledgements

We wish to express our gratitude to Dr Masao Tokita, Mr Nobuo Kanazawa and Mr Masakazu Kawahara of Sumitomo Coal Mining Co., Ltd for their help with spark-plasma-sintering. Thanks are also due to Dr Katsuhiro Nomura of Osaka National Research Institute for assistance with a.c. impedance spectroscopy measurements.

References

1. J. NOWOTNY and M. REKAS, *Key Engng Mater*. **66/67** (1992) 45.
2. R. BACSA, P. RAVINDRANATHAN and J. P. DOUGHERTY, *Mater. Res. Soc. Symp. Proc*. **243** (1992) 431.
3. E. SHI, C. R. CHO, M. S. JANG, S. Y. JEONG and H. J. KIM, *J. Mater. Res*. **9** (1994) 2914.
4. A. T. CHIEN, J. S. SPECK, F. F. LANGE, A. C. DAYKIN and C. G. LEVI, *ibid.* **10** (1995) 1784.
5. C.-R. CHO, E. SHI, M.-S. JANG, S.-Y. JEONG and S.-C. KIM, *Jpn. J. Appl. Phys*. **33** (1994) 4984.
6. K. KINOSHITA and A. YAMAJI, *J. Appl. Phys*. **47** (1976) 371.
7. D. HENNINGS, *Int. J. High Technol. Ceram*. **3** (1987) 91.
8. A. S. SHAIKH, R. W. VEST and G. M. VEST, *IEEE Trans. Ultraso. Ferroelec. Frequency Control* **36** (1989) 407.
9. G. CABOCHE and J. C. NIEPCE, in "*Ceramic Transactions*," Vol. 32, "Dielectric Ceramics: Processing, Properties and Applications," edited by K. M. NAIR, J. P. GUHA and A. OKAMOTO (American Ceramic Society, Westerville, OH, 1993) p. 339.
10. T. OTA, J. TAKAHASHI and I. YAMAI, *Key Engng Mater*. **66/67** (1992) 185.
11. K. OONISHI, T. MOROHASHI and K. UCHINO, *J. Ceram. Soc. Jpn* **97** (1989) 473.
12. W. R. BUESSEM, L. E. CROSS and A. K. GOSWAMI, *J. Amer. Ceram. Soc*. **49** (1966) 36.
13. G. A. SAMARA, *Phys. Rev*. **151** (1966) 378.
14. M. TOKITA, *J. Soc. Powder Technol Jpn* **30** (1993) 790.
15. I. KONDOH, T. TANAKA and N. TAMARI, *J. Ceram. Soc. Jpn* **102**, (1994) 505.
16. N. TAMARI, T. TANAKA, K. TANAKA, I. KONDOH, M. KAWAHARA and M. TOKITA, *ibid.* **103** (1995) 740.
17. N. HIROSE and A. R. WEST, *J. Amer. Ceram. Soc*. **79** (1996) 1633.
18. S. NAKA, F. NAKAKITA, Y. SUWA and M. INAGAKI, *Bull. Chem. Soc. Jpn* **47** (1974) 1168.
19. T. TAKEUCHI, K. ADO, Y. SAITO, M. TABUCHI, C. MASQUELIER and O. NAKAMURA, *Solid State Ionics* **79** (1995) 325.
20. S. SUMI, Y. MIZUTANI and M. YONEYA, *J. Jpn Soc. Powder Powder Metall.* **45** (1998) 153.
21. JCPDS Powder diffraction file, 5-626.
22. G. BUSCA, V. BUSCAGLIA, M. LEONI and P. NANNI, *Chem. Mater.* **6** (1994) 955.
23. J. JAVADPOUR and N. G. EROR, *J. Amer. Ceram. Soc*. **71** (1988) 206.

24. J. R. MACDONALD, "*Impedance Spectroscopy*" (Wiley, New York, 1987).
25. W. S. BAER, *J. Phys. Chem. Solids* **28** (1967) 677.
26. Y. SUYAMA and M. NAGASAWA, *J. Amer. Ceram. Soc.* **77** (1994) 603.
27. T. TAKEUCHI, M. TABUCHI, K. ADO, K. HONJO, O. NAKAMURA, H. KAGEYAMA, Y. SUYAMA, N. OHTORI and M. NAGASAWA, *J. Mater. Sci.* **32** (1997) 4053.

Received 1 June
and accepted 17 August 1998